Chemical Engineering Research and Design 222 (2025) 1–14

Contents lists available at ScienceDirect

Chemical Engineering Research and Design

journal homepage: www.elsevier.com/locate/cherd

Synthesis of higher alcohols from syngas: Exploring the parameter space and conceptual process design

Atte Aho [a], Marjut Suomalainen [b], Anssi Peuronen [c], Hannu I. Mikkonen [b], Niko Heikkinen [b], Päivi Mäki-Arvela [a], Irina Simakova [a], Kari Eränen [a], Mika Lastusaari [c], Juha Lehtonen [b], Dmitry Yu. Murzin [a,*]

[a] Laboratory of Industrial Chemistry and Reaction Engineering, Johan Gadolin Process Chemistry Centre, Åbo Akademi University, Åbo, Finland
[b] VTT Technical Research Centre of Finland Ltd., PL 1000, 02044 VTT, Finland
[c] Department of Chemistry, Intelligent Materials Chemistry Group, University of Turku, Finland

ARTICLE INFO

Keywords:
Higher alcohols
Syngas
Process design

ABSTRACT

Different reaction conditions were evaluated in the synthesis of higher alcohols over an 11 %-CuFeCoK/SiO_2 catalyst. The temperature range tested was 250–300 °C, pressure 10–30 bar, and the gas hourly space velocity of 1000–3000 mL $h^{-1}g_{cat}^{-1}$ all under a constant H_2:CO ratio of 2. At low CO conversions it was possible to achieve high selectivity to alcohols, while at high conversions side reactions forming CO_2 and alkanes became more dominating. Based on the experimental work, conceptual process design for alcohol production was conducted considering the main product, the aqueous alcohol mixture, and a gaseous by-product. The composition of the gaseous by-product had a H_2:CO molar ratio of 2, making it suitable for downstream Fischer-Tropsch and/or methanol synthesis, and a low content of other compounds. Due to high alcohol selectivity only at low CO conversion, recycling of the gases was taken into account in the conceptual process design and it was found that by recycling 98 % of the absorbed CO_2 and 70 % of the gaseous by-products a 50 % electricity demand and 20 % reactor volume decrease could be achieved.

1. Introduction

Higher alcohols, typically defined as alcohols with two or more carbon atoms in the structure (Luk et al., 2018), can be applied in the fine chemistry and energy sectors. Ethanol and isobutanol are usually produced through fermentation of glucose (Luk et al., 2017), while alcohols with more carbon atoms than in ethanol and isobutanol are on the other hand generally obtained through acid catalysed hydration of the corresponding alkenes (Luk et al., 2017). Higher alcohols can also be produced via the syngas route (Luk et al., 2017), however, not only alcohols are formed in higher alcohol synthesis (HAS) but also alkanes, alkenes and CO_2 through the water gas shift reaction (WGSR) according to the reactions below:

$n{\cdot}CO + 2n{\cdot}H_2 \rightarrow C_nH_{2n+1}OH + (n\text{-}1){\cdot}H_2O$, alcohols

$n{\cdot}CO + (2n+1){\cdot}H_2 \rightarrow C_nH_{2n+2} + n{\cdot}H_2O$, alkanes

$n{\cdot}CO + 2n{\cdot}H_2 \rightarrow C_nH_{2n} + n{\cdot}H_2O$, alkenes

$CO + H_2O \leftrightarrow CO_2 + H_2$, water gas shift reaction

Several different types of catalysts have been evaluated for the HAS from syngas. Typically four families of catalysts are active in HAS, namely Rh-based, Mo-based, CuCo and CuFe modified Fischer-Tropsch (FT) and methanol synthesis catalysts (Lind et al., 2024; Liu et al., 2019; Luk et al., 2017; Mäki-Arvela et al., 2022). Out of these types the CuFe-modified Fischer-Tropsch catalyst is considered the most promising catalyst due to the lower price of the active metals, high activity and selectivity to higher alcohols (Liu et al., 2019; Lu et al., 2012).

Typical reaction conditions for HAS are (Luk et al., 2017): temperature 130–360 °C, pressure 1–100 bar, gas hourly space velocity (GHSV) 1700–12000h^{-1} and H_2:CO ratio 1.0–2.9 depending on the catalyst used, i.e. extremely wide range of conditions have been reported. For the Cu-modified FT catalysts the conditions are more narrow, being for temperature 200–350 °C, pressure 20–70 bar, GHSV 3000–10000 h^{-1} and H_2:CO = 1–2 (Luk et al., 2017). The literature is scarce on papers reporting HAS results obtained at wide reaction conditions viz. at

* Corresponding author.
E-mail address: dmitry.murzin@abo.fi (D.Yu. Murzin).

https://doi.org/10.1016/j.cherd.2025.08.038
Received 4 July 2025; Received in revised form 15 August 2025; Accepted 20 August 2025
Available online 29 August 2025

different temperatures, pressures, GHSVs and H_2:CO ratios (Göbel et al., 2021; Luk et al., 2018). Typically, catalyst screening results are published just at singular reaction conditions (Chen et al., 2022; Hong et al., 2024; Liu et al., 2021; Xiao et al., 2013). Comparison of screening results is therefore, not straightforward as the selectivity to the possible HAS products can be strongly affected by the CO conversion, as has been shown earlier (Aho et al., 2024).

The effect of reaction temperature has been investigated in a number of papers (Aho et al., 2024; Göbel et al., 2021; Maximov et al., 2020). Maximov et al. (2020) performed HAS at four different temperatures namely, 300, 320, 340 and 360 °C at a constant 5 MPa pressure and 760 mL h^{-1} g_{cat}^{-1} using several metal-modified (Fe, Co, Ni) MoS_2/Al_2O_3 catalysts in both un-promoted and K-promoted states. The authors (Maximov et al., 2020) reported that CO conversion was enhanced at higher reaction temperatures, as expected, however, an in-depth selectivity break-down of the different products formed at all tested temperatures was not provided. Potassium promotion had a retarding effect on the CO conversion for the MoS_2/Al_2O_3 and $FeMoS_2/Al_2O_3$, while an increase in conversion was observed for the Co and Ni modified MoS_2/Al_2O_3 catalysts. The catalyst promotion with potassium had a positive effect on the HAS product distribution in a way that less hydrocarbons were formed and more of the liquid product. Moreover, the distribution of alcohols changed with decreasing significantly selectivity to the undesired methanol while improving selectivity to C_{2+} alcohols (Maximov et al., 2020).

The influence of reaction pressure has been studied in refs. (Göbel et al., 2021; Li et al., 2020; Luk et al., 2018). Göbel et al. (2021) investigated the influence of the reaction pressure by carrying out experiments at 15, 30, 45 and 60 bar. The authors (Göbel et al., 2021) observed that the CO conversion increased linearly with increasing pressure. Interestingly, the product distribution was only slightly influenced within a higher, 30–60 bar, pressure range in a way that the selectivity to olefins decreased (Göbel et al., 2021). At the lowest pressure tested, 15 bar, the selectivity to hydrocarbons and CO_2 increased compared to higher pressures, simultaneously decreasing the corresponding values of the alcohols (Göbel et al., 2021). In Göbel et al. (2021) also the effect of partial pressure of CO and H_2 in the H_2:CO range of 0.50–2.67 at a constant 60 bar pressure including 12–27 bar of N_2 was studied. It was reported (Göbel et al., 2021) that CO conversion increased with an increased H_2:CO ratio and that the selectivity to methanol increased at a lower CO partial pressure.

In order to compare different HAS catalysts in a fair way Luk et al. (2019) adjusted the GHSV, between 4000 and 34000 mL h^{-1} g_{cat}^{-1}, to obtain a CO conversion of 4 % keeping the reaction temperature at 270 °C, pressure at 5 MPa and H_2:CO ratio equal to 2. The authors (Luk et al., 2019) studied the influence of carrier acidity of CuFe catalysts by using MFI as the support with different Si/Al ratio, namely, 15, 40 and 140 as well as the pristine silicalite. The impact of potassium promotion was also included in the scope of Luk et al. (2019). The least acidic materials, i.e. MFI with the highest Si/Al ratio and the silicalite itself, afforded the highest selectivity to primary alcohols while more acidic supports generated also secondary alcohols as well as dimethyl ether. However, roughly 60 % of alkanes, alkenes and CO_2 were formed at a considerably low CO conversion (Luk et al., 2019).

Our group recently studied the influence of Cu:Fe ratio of CuFeCoK/attapulgite catalysts in synthesis of higher alcohols from syngas (Aho et al., 2024) at different reaction temperatures, ranging from 225 to 300 °C, and at two different H_2:CO ratios, namely 1 and 2, while the pressure was kept constant at 30 bar. It was reported (Aho et al., 2024) that the Cu:Fe ratio influenced the reaction in a way that a higher iron content catalyst was more active in syngas conversion and had a higher selectivity to higher alcohols than the other catalysts. Moreover, a higher H_2:CO ratio and higher reaction temperature increased the conversion. However, it was found that the selectivity to the liquid products decreased as the conversion of CO increased and furthermore, a higher selectivity to CO_2 and alkanes was obtained (Aho et al., 2024).

In this work the influence of process parameters, such as temperature, pressure, gas hourly space velocity, on the syngas transformation to higher alcohols was studied over an affordable 11 % CuFeCoK/SiO_2 catalyst. Generation of such data allowed development of a conceptual process design for producing higher alcohols from carbon dioxide and renewable hydrogen via synthesis gas. The conceptual process design here concentrates on evaluating the effect of gas recycling to technical performance, thus differing from our previous work (Vikram et al., 2025) where the syngas was derived from biomass gasification and the main focus was on sensitivity analysis and predominantly separation of alcohols. Herein technical feasibility of the designed alcohol production concepts was assessed based on calculated mass and energy balances. Further processing options of both main product stream and by-product stream were discussed.

2. Experimental

2.1. Catalyst preparation

The 11CuFeCoK/SiO_2 catalyst used in this work was containing 6 wt % Cu, 4 wt% Fe, 0.5 wt% Co, 0.5 wt% K and was synthesized by the incipient wetness impregnation of silica (Sigma Aldrich, Davisil Grade 62). An aqueous mixture of active phase precursors such as Cu$(NO_3)_2{\cdot}3\,H_2O$ (Reachim, 98 %), Fe$(NO_3)_3{\cdot}9\,H_2O$ (Sigma Aldrich, 99 %), Co$(NO_3)_2{\cdot}6\,H_2O$ (Reachim, 98 %) and KNO_3 (Reachim, 98 %) was added to the preliminary dried silica powder (100 °C, 17 h) at room temperature. Thereafter, this sample was dried in oven under at 100 °C (17 h) and calcinated in air flow at 450 °C (6 h) with the temperature ramp 2 °C/min.

2.2. Catalyst characterization

N_2-physisorption to determine the specific surface area and pore size distribution was performed with a Micromeritics 3D-Flex instrument. Prior to the measurements the catalyst samples were dried ex-situ at 180 °C over-night and in-situ at 250 °C for 4 h. The BET equation was used for calculating the specific surface and Horwath-Kawazoe method for the pore volume and size distribution.

CO DRIFTS measurements were performed with a Shimadzu IRTracer-100 spectrometer equipped with a high-temperature environmental chamber and DRIFTS collector (Spectra-Tech Inc.). Gas lines for N_2, H_2 and CO were connected to the water-cooled cell. The experiments were carried out by placing a small amount of the catalyst powder in the sample holder of the cell, thereafter, the lid of the cell was attached and after a short N_2-flush the cooling of the cell wall was started. The catalyst sample was reduced at 300 °C in a 10 mL/min flow of hydrogen (Woikoski, N50) for 30 min. After the reduction, the cell was flushed with 10 mL/min flow of nitrogen (Woikoski, N50) before cooling down to the desired temperature. A background spectrum was recorded at room temperature and thereafter the gas composition was changed to include 10 % CO (Air Liquide, 3.7) in nitrogen (Woikoski, N50) keeping the same 10 mL/min total flow. The catalyst surface was saturated with CO for 15 min and then the flow of CO was discontinued. The spectrum was recorded immediately at 0 min when starting CO adsorption and thereafter at 5, 10, and 15 min and continued during desorption at 5, 10, 20 and 30 min.

Temperature programmed reduction (TPR) was studied with a Microtrac MRB, Belcat II device. The catalyst sample (50 mg) was dried in the sample holder tube at 300 °C in a 30 mL/min flow of argon. TPR was carried out from 35 °C to 800 °C with a heating rate of 10 °C/min in a 30 mL/min flow of 5 % hydrogen in argon.

The powder X-ray diffraction data were collected with Malvern PANalytical Aeris Research Edition diffractometer, equipped with PIXcel1D detector, by using Cu $K_{\alpha1,\alpha2}$ radiation (40 kV, 7.5 mA). The samples were prepared onto Si zero-background disc and were rotated 60 rpm during the data collection. Pulse Height Discrimination (PHD)

settings of 7.8 kV for the low and 11.3 kV for the high limit to alleviate issues arising from X-ray fluorescence due to Cu X-ray source and presence of Fe and small amount of Co in the samples. The phase identification was done within HighScore Plus v4.9 software (Degen et al., 2014) using PDF-4 + database (Gates-Rector and Blanton, 2019).

2.3. Reactor set-up and experimental procedure

A stainless steel tube with an inner diameter of 6 mm and a total length of 35 cm was used as the higher alcohols synthesis reactor. The tube was placed in an aluminium block inside the oven (Carbolite) to ensure better heat transfer. K-type thermocouples monitored the temperature of the oven and the catalyst bed. The gas flows of hydrogen (Woikoski N50), carbon monoxide (Air Liquide 3.7) and nitrogen (Woikoski N50) were controlled by the Brooks Instrument mass flow controllers (MFC). Nitrogen was used as an internal standard in the flow calculations. The pressure in the set-up was controlled with a back-pressure regulator (Equilibar). Downstream the regulator, the formed alcohols were condensed at −15 °C and the gases eluting through the condenser were analyzed by an on-line GC (HP 6890 Series) equipped with both HP-PLOT-Q and HP-MOLSIV columns as well as TC and FI detectors for separation and analysis of CO, H_2, N_2, C1-C6 alkanes and C2-C6 alkenes along with CO_2. A scheme of the set-up is displayed in Fig. 1.

The reactor tube was filled by packing quartz wool in the bottom followed by glass beads (Sigma, 425 – 600 μm) to get the catalyst bed approximately to the middle height of the tube. The catalyst (0.5 g, 125 – 250 μm) was diluted with the equal amount of the glass beads and finally the remaining part of the tube was filled with glass beads. Between every bed a thin layer of quartz wool was used to avoid mixing of the materials.

The set-up was pressurized with nitrogen and carefully checked for possible leakages. When it was ensured that no leakage was present, the pressure was released to atmospheric one. The catalyst was reduced for 3 h in 10 mL/min (STP) hydrogen flow followed by carburization for 3 h with 10 mL/min (STP) CO flow at 300 °C before starting the synthesis of higher alcohols. It has been reported (Luo et al., 2009) that carburization with CO increases the CO conversion in FT synthesis with a low alpha iron catalysts as the transformation of iron into χ-Fe_5C_2 is enhanced compared to other pretreatment methods. Iron carbides have been reported to act as the active sites for CO dissociation and chain propagation (Zeng et al., 2021). After carburization the gas was switched to nitrogen and the temperature was lowered to 250 °C.

After the pretreatment, different reaction condition were tested namely, GHSV of 1000, 2000 and 3000 $mL_{gas}\ h^{-1}\ g_{cat}^{-1}$, pressure of 10, 20 and 30 bar at GHSV 2000, temperature of 250, 275 and 300 °C at all pressures and GHSV, the H_2:CO ratio was kept constant at 2 and the concentration of N_2 used as the internal standard constant, as well, at 6 %. The different reaction conditions are displayed in Fig. 2 as a function of time-on-stream.

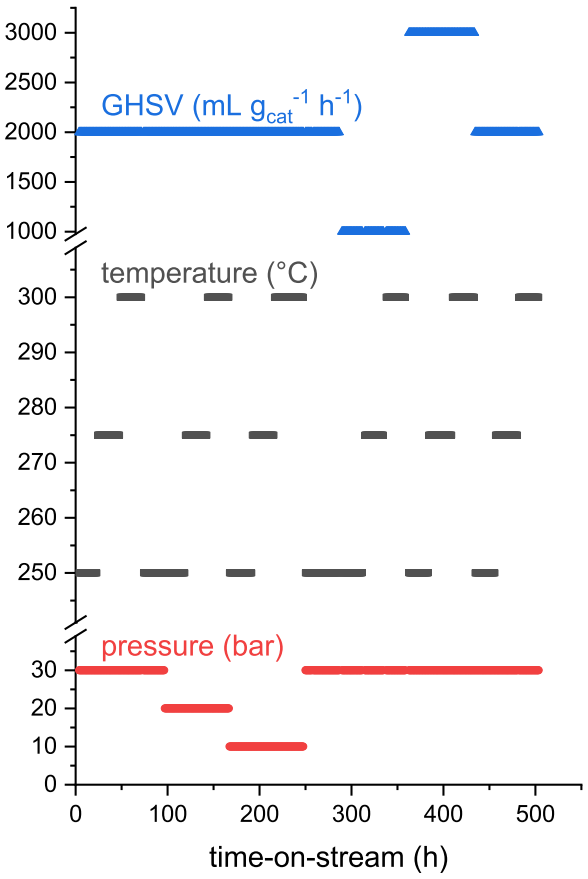

Fig. 2. Reaction conditions tested, including pressure (bar), temperature (°C) and gas hourly space velocity (mL $g_{cat}^{-1}\ h^{-1}$) as a function of time-on-stream.

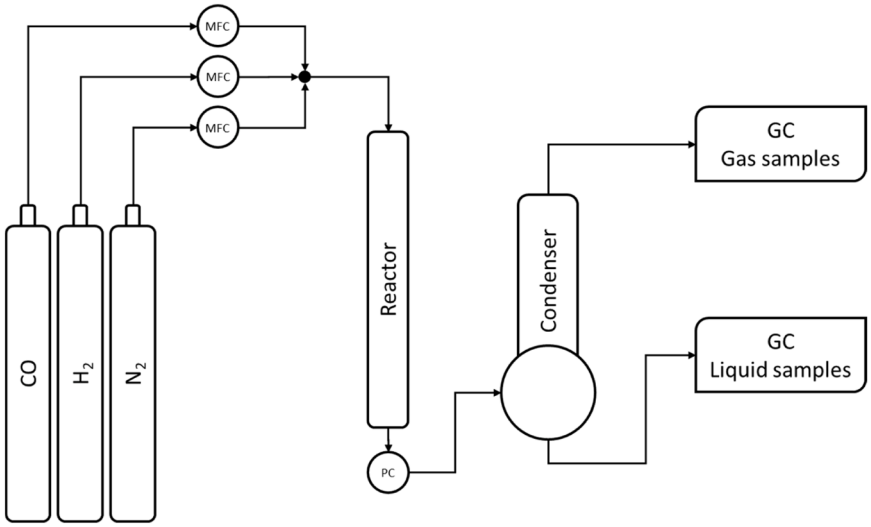

Fig. 1. Reactor set-up scheme.

2.4. Product analysis

Online analysis of the eluting gas stream was done with the GC described above. The responses from TC and FI detectors were calibrated for CO_2, n-alkanes ranging from methane to hexane and linear α-olefins ranging from ethene to hexene.

The collected liquid product was analysed by GC (HP 6890 Series). Separation of the alcohols was done in a FFAP column using the following temperature program, 2 min at 50 °C, heating to 220 °C with 5 °C/min and holding for 10 min. The flame ionization detector was calibrated for linear primary alcohols starting from methanol all the way up to 1-decanol.

2.5. Conceptual process design

A concept for producing alcohols from CO_2 and renewable hydrogen via synthesis gas based on experimental data was developed. Mass and energy balances were calculated using Aspen Plus simulation software for the developed process concept, based on the selected results from the experimental data. Property method used in simulation was Soave Redlich Kwong (SRK) equation of state, except for the solid liquid separation, which was modelled using cubic-plus-association (CPA). When no experimental data were available, operation and performance parameters were based on the literature or in house experience.

3. Results and discussion

3.1. Catalyst characterization results

The nitrogen physisorption isotherm for the fresh catalyst displayed in Fig. 3, gives the specific surface area as calculated with the BET equation equal to 156 m^2/g. The total pore volume was 0.62 mL/g_{cat}, calculated with the Horvath-Kawazoe method, and the pore size distribution showed the presence of both micropores, < 2 nm, and mesopores 2 – 50 nm.

Fig. 4 shows the DRIFTS spectra during CO adsorption 0–15 min and CO desorption 0–30 min. The absorbance peaks at 2171 and 2119 cm^{-1} are most likely due to the gas-phase CO as reported by refs. Sonal et al. (2020) and Wu et al. (2015). CO can adsorb linearly on Cu^+ sites forming a Cu^+-carbonyl, visible after flushing away the gaseous CO with an inter gas, at the principle band 2120–2136 cm^{-1} as reported by several authors (Hornés et al., 2009; Subramanian et al., 2012). CO can also be adsorbed on highly dispersed Cu^0 sites at the same frequency as the Cu^+-CO, however, the stability of this bond is usually weak and easily broken during desorption (Subramanian et al., 2012). No peaks could be observed during desorption of CO indicating that CO is very weakly bound to the surface and that the copper is probably mainly present as metallic copper, as reported earlier based on XPS analysis of a similar type of catalyst (Aho et al., 2024). Moreover, it has been suggested (Gong et al., 2023) that a weakened CO adsorption on metal surfaces suppresses the C-O cleavage which could be beneficial for CO insertion reactions as they are essential for formation of higher alcohols from syngas.

Fig. 5 shows the reduction behaviour of the tested 11 %-CuFeCoK/SiO_2 catalyst. Three different peaks can be observed, the peak below 300 °C originates probably from the reduction of highly dispersed CuO, while the peak above 300 °C is most likely due to reduction of larger CuO particles as reported in Aho et al. (2024) and He et al. (2006). The last peak with a maximum TPR signal at approximately 550 °C corresponds to the reduction of Fe (Khunphonoi et al., 2022).

The recorded powder X-ray diffraction patterns of reduced (3 h 300 °C in hydrogen atmosphere), as prepared (calcined) and spent 11 %-CuFeCoK/SiO_2 catalyst are shown in Fig. 6. The reduced catalyst (Fig. 6a) shows broad amorphous features of the supporting material while peaks with weak intensity can be distinguished from the recorded pattern that can be attributed to different metal (M^0) and metal oxide

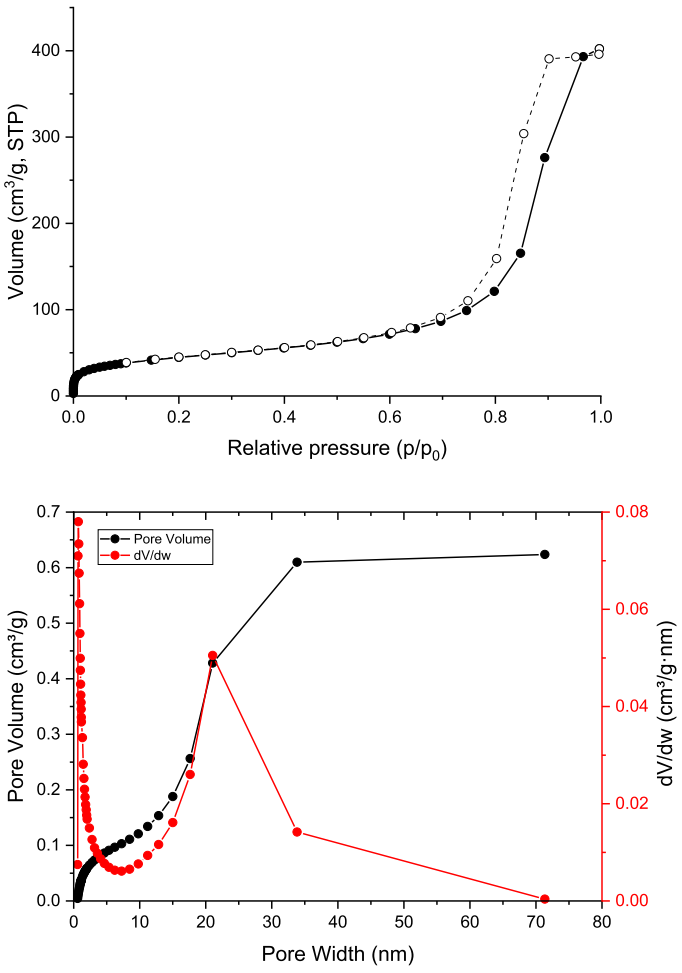

Fig. 3. Textural properties characterization: a) nitrogen adsorption isotherm for the 11CuFeCoK/SiO_2 catalyst with closed and open symbols representing respectively adsorption and desorption, b) pore size distribution.

phases. The material possibly contains both Cu^0 (PDF 00–004–0836) and α-Fe^0 (PDF 04–007–9753) as metallic phases although their identification is based on very weak peaks at 43.3° and 50.4° (2θ), and 44.7° (2 θ), respectively. With regards to the oxide phases, the calculated peaks of Cu_2O (PDF 03–065–3288), FeO (PDF 01–089–0687) and Fe_3O_4 (PDF 01–078–6086) fit the barely distinguishable features in the diffractogram of reduced 11 %-CuFeCoK/SiO_2 catalyst as pointed in Fig. 6a. The calcined sample (Fig. 6b) shows peaks of two different crystalline phases. These are assigned as $CuFe_2O_4$ (PDF 04–026–3795), which is a spinel phase with a smaller unit cell ($a = 8.21$ Å) compared to Fe_3O_4 ($a = 8.49$ Å), and α-Fe_2O_3 (PDF 04–008–8479). Cobalt is not observed as a separate phase as it is most likely mixed into the two metal oxide phases or is undetectable due to its small amount in the sample. The XRD pattern of the spent catalyst (Fig. 6c) contains peaks of Cu^0 phase (PDF 00–004–0836, $a = 3.62$ Å) which is also consistent with the γ-Fe^0 (austenite) phase. The presence of pure Fe^0 in this phase is highly unlikely due to its phase transition to α-Fe below 912 °C. Therefore, Fe^0 either exists as a Fe-Cu solid solution or is stabilized by a small amount of carbon resulting from the catalytic reaction. The crystallite size of the metal phase was calculated using the Scherrer equation being ca. 15 nm. It is worth noting that the diminutive peak at 59.82° 2θ emerges in the diffractogram during the last repetition of the data collection and is most likely a spurious peak rather than oxidation of the sample due to atmospheric oxygen.

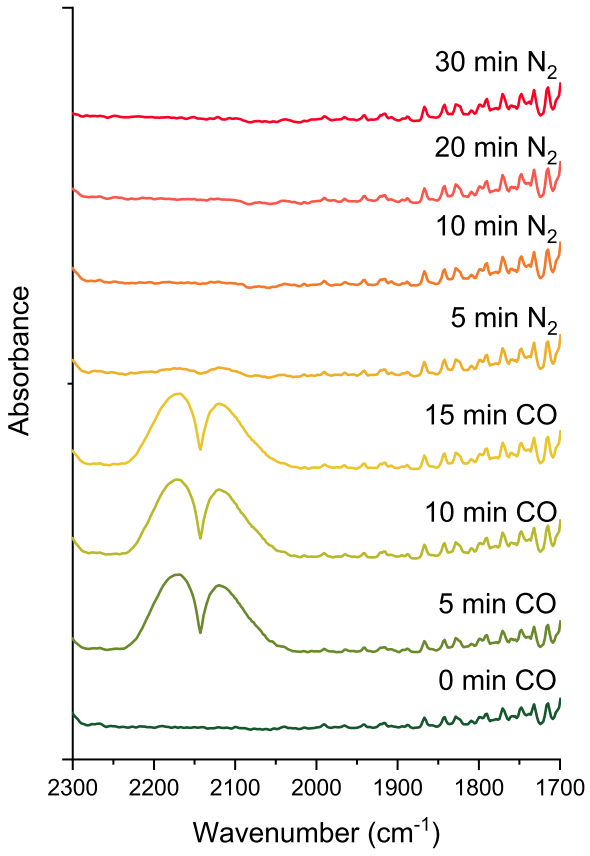

Fig. 4. CO DRIFTS results for 11 %-CuFeCoK/SiO_2 catalyst.

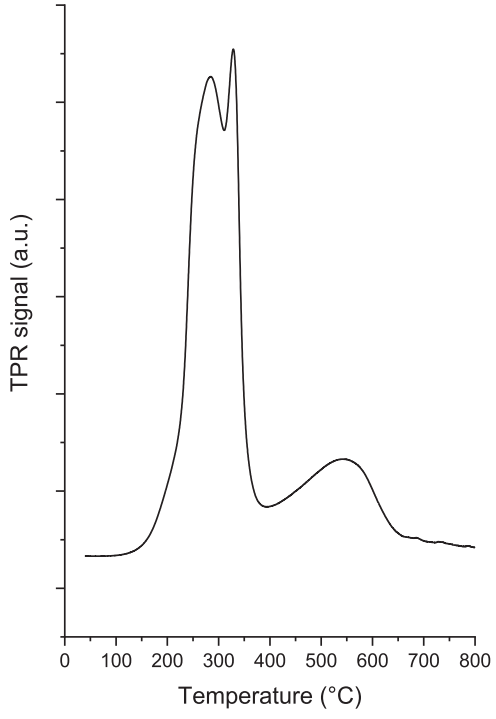

Fig. 5. Temperature programmed reduction profile of the 11 %-CuFeCoK/SiO_2 catalyst.

3.2. Catalytic results

The total duration of testing of different reaction conditions was over 500 h. The CO conversion as a function of time-on-stream at the various reaction conditions is displayed in Fig. 7.

From Fig. 7 it can be observed that the steady state was not reached at the highest reaction temperatures, showing a decline in CO conversion. Moreover, comparing the last reaction cycle starting at 434.5 h, having the same reaction conditions as in the beginning of the experiment (30 bar, 2000 h^{-1} g_{cat}^{-1}), it can be noted that the conversion of CO is higher in the beginning of the experiment at 250 °C than at 434.5 h. However, comparing the 5 last CO conversion points at 300 °C the average conversion was 75.4 % in the first cycle and 75.0 % in the second cycle, the results reported later in the paper are based on the average from 10 last data points before changing the reaction conditions. It can be concluded that while some catalyst deactivation is observed during the $>$ 500 h of testing, a better picture of catalyst deactivation would require prolonged testing at pilot conditions under the influence of mass transfer for a significantly longer period than what was applied in this work.

The conversion of CO and H_2 at different GHSV (at a constant pressure of 30 bar) and pressures (at a constant GHSV of 2000 mL_{gas} h^{-1} g_{cat}^{-1}) as a function of reaction temperature is displayed in Fig. 8 and Fig. 9.

From Fig. 8 and Fig. 9 it can be observed that the conversions increases with temperature, as expected, and with pressure, while it decreases upon increasing GHSV due to shorter residence time. The pressure dependence on the conversion can be attributed to the residence time as the GHSV is defined at standard temperature and pressure and thus the reaction pressure influences the residence time of the gases in the reactor in a way that it is shorter at lower pressures and thereby the conversion seems to be lower at lower pressures. A decrease in conversion at lower pressures, in the tested range 2–4 MPa, has also been reported in the Fischer-Tropsch (FT) synthesis using a Co/SiO_2 catalyst changing also the product distribution in a way that more of C_{6+} products were formed at a higher pressure and higher CO conversion (de la Peña O'Shea et al., 2005).

The reaction rates for CO and H_2 calculated from the conversions shown in Fig. 8 and Fig. 9 are listed in Table 1. The apparent activation energies calculated based on the reaction rates are plotted as a function of pressure and GHSV in Fig. 10.

From Table 1 it is possible to calculate the ratio between the reaction rates for hydrogen and CO giving the values ca. between 1.5 and 2.0, which is not consistent with the reactions forming the alcohols, alkanes and alkenes mentioned in the Introduction. However, by taking into account the WGSR consuming CO and generating H_2 the ratio falls in most cases between 2 and 3, which corresponds well with the stoichiometric factors for hydrogen in the reactions taking place.

Interestingly, it seems that the apparent activation energy plotted in Fig. 10a increases with pressure while different GHSV, Fig. 10b, result in a more or less constant apparent activation energy within the reaction conditions tested. A possible reason for the increasing apparent activation energy with pressure could be presence of mass transfer constraints at lower pressures, or a complex reaction mechanism for which the apparent activation energy depends on the frequencies of steps. The latter depend on the pressure as reported in for example (Murzin, 2019).

The reaction orders for CO and H_2 were determined from a power-law model by varying the total pressure in the reactor. The linearized logarithmic plots for the reaction rates for CO and H_2 as a function of their pressures are illustrated in Fig. 11. Based on the slopes in Fig. 11 the reaction order for CO is between 0.5 and 1 and for H_2 between 0.8 and 1.1. The reaction order for H_2 is comparable to the results reported by Göbel et al. (2021), while the order for CO differs significantly as in Göbel et al. (2021) a zero order on CO pressure was reported with an apparent activation energy of 140 kJ/mol, which is slightly higher than the value reported here.

The water gas shift reaction is considered to be a side-reaction in the

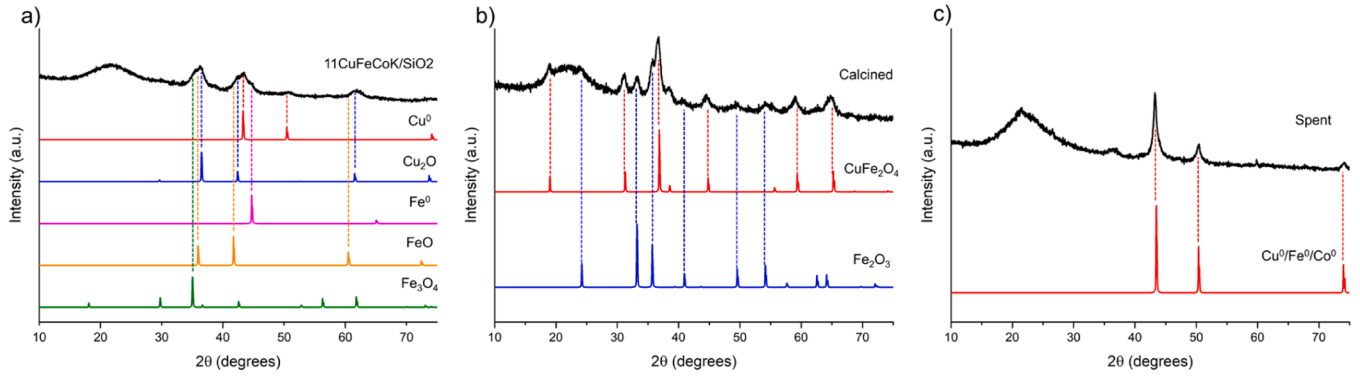

Fig. 6. XRD patterns (in black) of 11 %-CuFeCoK/SiO_2 catalyst recorded from a) reduced, b) calcined and c) spent catalyst samples.

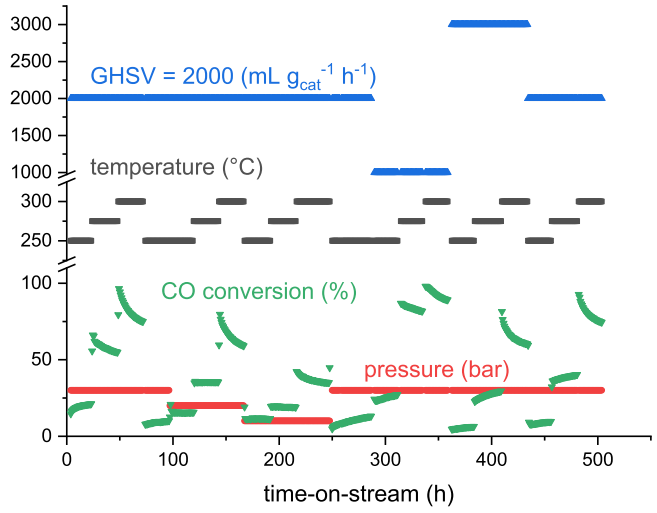

Fig. 7. Conversion of CO as a function of time-on-stream at different reaction conditions.

synthesis of higher alcohols. The selectivity to CO_2 as a function of CO conversion (temperatures 250, 275 and 300 °) is plotted in Fig. 12. The reaction conditions 30 bar and GHSV 2000 g_{cat}^{-1} h^{-1} were repeated, denoted as "rep" in Fig. 12.

From Fig. 12 it can be concluded that the selectivity to CO_2 is essentially independent on reaction temperature, pressure and GHSV, increasing with CO conversion and reaching selectivity of over 40 % at almost complete conversion. Consequently, at low CO conversion levels the selectivity to CO_2 is almost negligible being as low as approximately 4 % at 12 % conversion at the lowest reaction pressure. It has been reported that CO_2 selectivity is increasing with metal particle size (Luk et al., 2018).

Selectivity to the gas phase alkanes and alkenes at different reaction conditions along with the CO conversion is listed in Table 2 and Table 3.

From Table 2 and Table 3 it can be concluded that the selectivity to gas phase alkanes increases with temperature, i.e. increased CO conversion, and pressure, while the GHSV has only a minor effect on the selectivity, however, an increasing trend can be observed for ethane and propane. The selectivity behaviour is opposite for the alkenes compared to the alkanes, as at higher reaction temperature and higher CO conversion levels less alkenes are generated.

The liquid product selectivity was calculated based on the difference from the sum of products in Table 2 and Table 3 taking into account the formation of CO_2 plotted in Fig. 12. The selectivity to alcohols calculated based on selectivity to both liquid products as well as concentrations from GC analysis is listed in Table 4.

Opposite to the alkane selectivity trends it can be observed from Table 4 that the selectivity to alcohols decreases with temperature (CO conversion) and that a lower reaction pressure yields higher selectivity compared to a higher pressure, moreover, a small increase in selectivity can be observed at higher GHSV compared to the lower one, here again the CO conversion is higher at lower GHSV. Similar trends for the selectivity dependence were observed, namely the selectivity to alkanes increases with CO conversion, while selectivity to alcohols and alkenes decreases with elevation of CO conversion using slightly different catalysts in the previous work of the authors (Aho et al., 2024).

The Anderson-Schulz-Flory (ASF) distribution was used to calculate α-values for the formed alcohols, alkanes and alkenes with the carbon numbers higher than two or three for the alkenes, with the α-values listed along with the coefficient of determination, R^2, in Table 5. The reason for evaluating the α-value for compounds with more than two or three carbon atoms in them is a poor correspondence of these compounds with the linear ASF plot, opposite to the C1 compounds, namely, methanol, methane and ethene as seen in a typical ASF plot illustrated in Fig. 13.

From Table 5 it is possible to calculate the average α-values for the alcohols (0.27), alkanes (0.46) and alkenes (0.39). Clear differences can be observed between the α-values for the different products indicating that they are formed through different reaction pathways. Deviations from the linear fit for the C_1 and C_2 products are also related to different mechanisms for synthesis of compounds with high carbon numbers through chain propagation, compared to C_1-C_3 products. Based on the α-values listed in Table 5 it can be observed that for the alcohols the α-value decreases with temperature independently on GHSV, no main trends can be observed at different reaction pressures. A reason for this dependency is that the rate constants for propagation and termination of alcohol formation are only dependent on the temperature and not pressure contrary to FT synthesis where not only temperature influences the α-value in the same way as in the current study but also pressure has an impact increasing it (Chen and Yang, 2019). For the alkanes the α-value can be considered more or less constant independent on pressure and GHSV at the tested temperature range. The clearest trend can be seen for the alkenes at different reaction pressures, displayed in Fig. 14, showing that at lower pressures more alkenes with a higher α-value are formed compared to higher pressures, a small decrease in the α-value with temperature can also be observed for all pressures tested.

The influence of reaction pressure on the α-value for alkenes has been observed previously in Fischer-Tropsch synthesis (Zheng et al., 2007). Zheng et al. (2007) studied the effect of pressure in FT synthesis using a 15 % Co/SiO_2 catalyst and varied the reaction pressure from 0.2 to 2.0 MPa. It was reported (Zheng et al., 2007) that the α-value linearly increased from ca. 0.83 to ca. 0.90 at 0.2–1.5 MPa, consistent with a decreased methane selectivity. Between 1.5 and 2.0 MPa only a slight increase in the alkene α-value was observed. The authors (Zheng et al., 2007) also reported that a higher reaction pressure increased the conversion and CO and H_2 similarly to results in Fig. 8 and Fig. 9. A probable

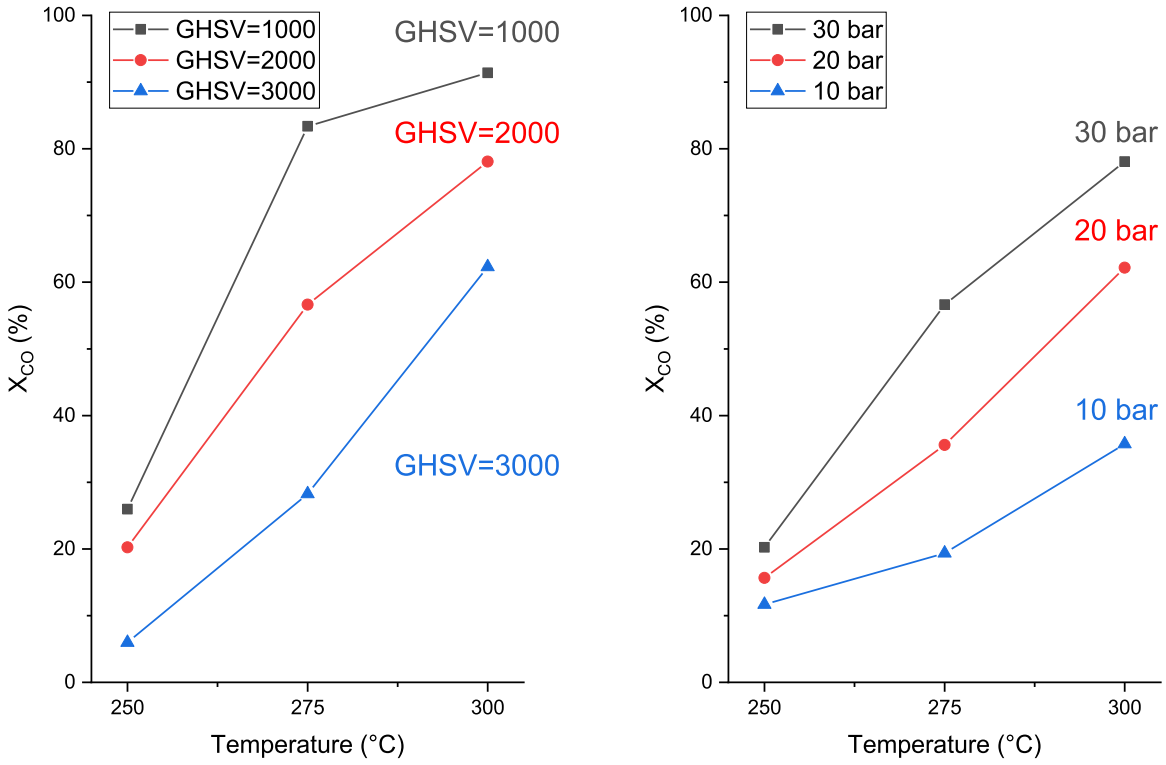

Fig. 8. Conversion of CO at different reaction pressures and GHSV as a function of temperature.

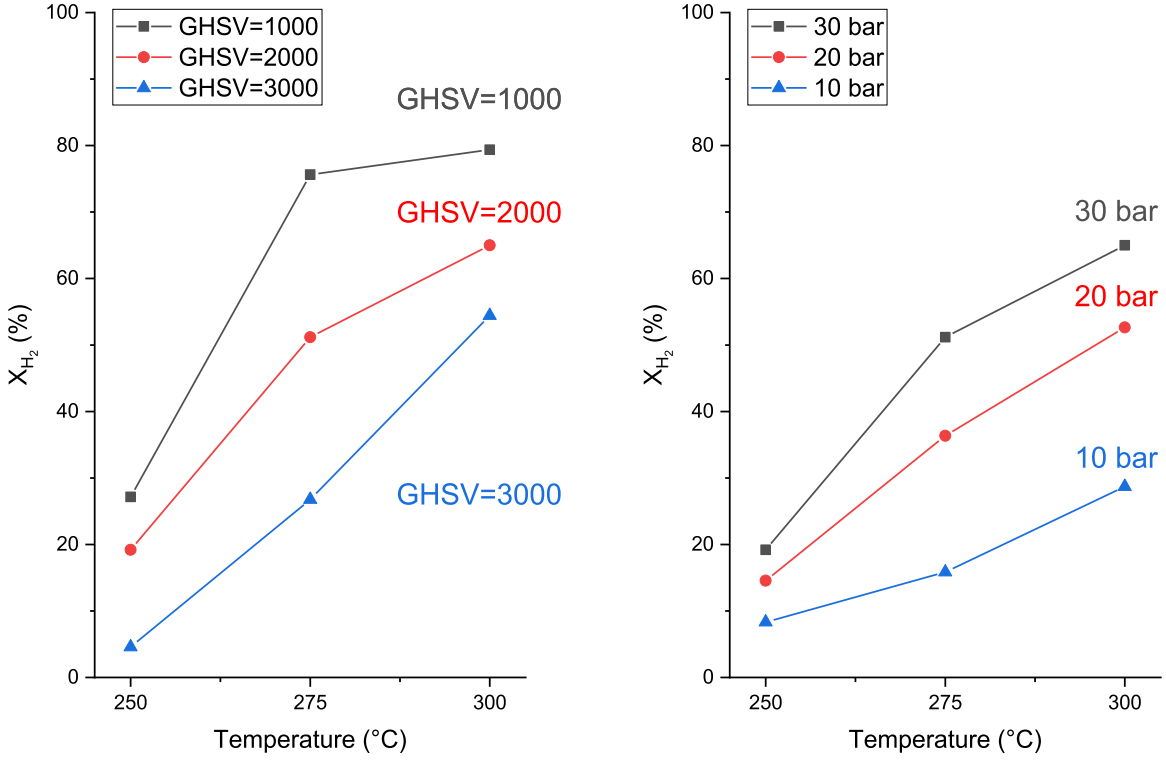

Fig. 9. Conversion of H_2 at different reaction pressures and GHSV as a function of temperature.

reason for the improved α-value in Zheng et al. (2007) was speculated to be a higher formation of C_1 intermediates at higher CO conversion which could increase the rate of propagation. The α-value results presented in Fig. 14 and CH_4 selectivity in Table 2 are opposite to the results of Zheng et al. (2007) and instead of chain propagation at higher pressure complete hydrogenation to alkanes occurred over the CuFe-CoK/SiO_2 catalyst used in this work.

Table 1
Reaction rates for CO and H_2 at different reaction conditions.

Temperature (°C)	Pressure (bar)	GHSV (mL/h g_{cat})	$-dn_{CO}/dt$ (μmol/g_{cat} s)	$-dn_{H2}/dt$ (μmol/g_{cat} s)
250	30	2000	0.79	1.49
	20	”	0.61	1.13
	10	”	0.45	0.65
275	30	”	2.20	3.98
	20	”	1.38	2.82
	10	”	0.75	1.23
300	30	”	3.03	5.05
	20	”	2.41	4.09
	10	”	1.39	2.23
250	30	3000	0.35	0.53
	”	2000	0.79	1.49
	”	1000	0.50	1.05
275	”	3000	1.65	3.12
	”	2000	2.20	3.98
	”	1000	1.62	2.94
300	”	3000	3.63	6.34
	”	2000	3.03	5.05
	”	1000	1.77	3.08

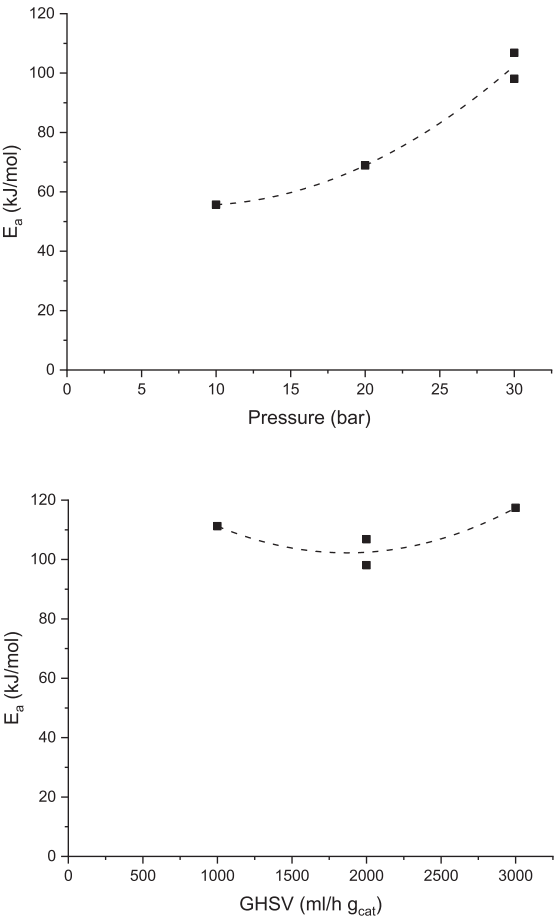

Fig. 10. Apparent activation energy as a function of a) pressure and b) GHSV.

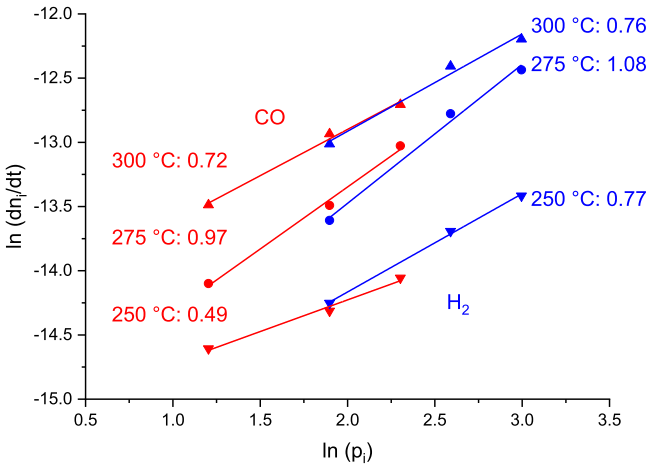

Fig. 11. Linearized logarithmic plots for CO and H_2 reaction rates as a function of their partial pressures.

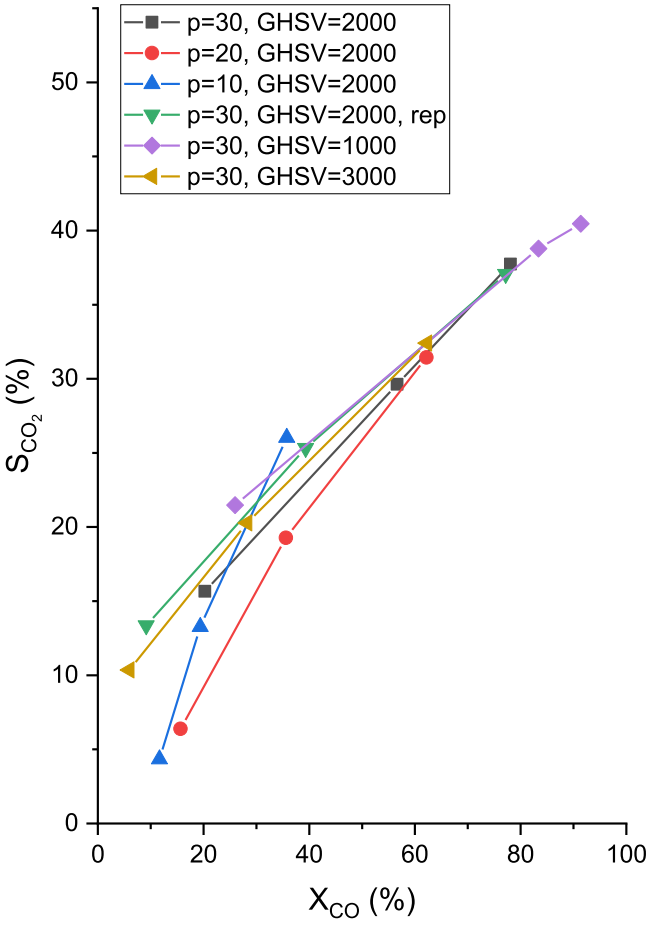

Fig. 12. Selectivity to CO_2 as a function of CO conversion at different reaction conditions.

3.3. Conceptual process design

The flowsheet of the developed concept for producing higher alcohols from CO_2 and green hydrogen via synthesis gas is presented in Fig. 15. Pressurised hydrogen and oxygen are produced from water by alkaline electrolyser (AEL). All of the AEL output hydrogen and part of the oxygen are utilized in the RWGS/CPOX process. CO_2 is compressed to the process pressure of 10 bar. Gases are heated up to 700 °C and directed to the RWGS/CPOX reactor, which operates at 850 °C and converts CO_2 to CO by reverse water-gas shift reaction (RWGS). The other possible reactions that may occur in the reactor (methane formation, methanation, hydrocarbon reforming, solid carbon formation) are considered by identifying all potential products and allowing the reactor to reach chemical equilibrium based on minimizing the Gibbs energy. The heat required for the endothermic RWGS reaction and final heating of the gases is provided by adding sufficient amount of oxygen in the feed, causing partial oxidation of hydrogen. After the RWGS/CPOX

Table 2
Selectivity to different alkanes at different reaction conditions.

Temperature (°C)	Pressure (bar)	GHSV (mL/h g_{cat})	X_{CO} (%)	methane (%)	ethane (%)	propane (%)	butane (%)	pentane (%)	hexane (%)
250	30	2000	20.3	22.0	6.8	3.4	2.4	1.6	0.9
	20	”	15.7	11.3	2.6	1.2	1.0	0.6	0.4
	10	”	11.7	6.8	0.9	0.5	0.5	0.0	0.0
275	30	”	56.6	22.3	9.0	3.7	2.4	1.7	1.1
	20	”	35.6	18.2	6.0	2.1	1.6	1.1	0.7
	10	”	19.4	14.4	3.2	1.0	0.9	0.6	0.5
300	30	”	78.1	25.2	8.9	4.1	2.1	1.9	1.2
	20	”	62.2	21.3	7.1	2.8	1.7	1.6	1.1
	10	”	35.7	18.8	5.0	1.5	1.1	1.1	0.8
250	30	3000	6.0	22.6	4.8	2.5	2.0	1.1	0.3
	”	2000	9.2	23.7	6.1	2.9	2.3	1.5	0.9
	”	1000	26.0	24.1	9.5	4.0	2.8	1.8	1.0
275	”	3000	28.2	23.9	8.6	3.0	2.1	1.4	0.8
	”	2000	39.3	23.6	9.1	3.3	2.4	1.6	1.0
	”	1000	83.4	23.6	10.4	6.0	3.0	2.4	1.1
300	”	3000	62.3	25.2	9.1	3.7	2.2	1.8	1.1
	”	2000	77.2	25.6	9.2	4.8	2.6	2.1	1.2
	”	1000	91.4	28.2	10.3	6.9	3.1	2.4	1.2

Table 3
Selectivity to different alkenes at different reaction conditions.

Temperature (°C)	Pressure (bar)	GHSV (mL/h g_{cat})	X_{CO} (%)	ethene (%)	propene (%)	butene (%)	pentene (%)	hexene (%)
250	30	2000	20.3	3.4	7.2	3.7	1.9	0.9
	20	”	15.7	2.4	3.6	2.2	1.0	0.6
	10	”	11.7	1.8	2.1	1.6	0.8	0.5
275	30	”	56.6	0.8	5.8	2.8	1.4	0.6
	20	”	35.6	1.5	5.2	2.9	1.5	0.8
	10	”	19.4	2.3	4.4	2.8	1.5	0.9
300	30	”	78.1	0.3	4.0	1.6	0.8	0.2
	20	”	62.2	0.6	4.4	2.1	1.1	0.5
	10	”	35.7	1.5	5.3	3.1	1.8	0.9
250	30	3000	6.0	5.9	7.0	4.3	1.9	1.1
	”	2000	9.2	4.8	7.5	4.6	2.3	1.4
	”	1000	26.0	2.3	7.8	4.3	2.1	1.0
275	”	3000	28.2	2.0	7.0	3.9	2.0	1.0
	”	2000	39.3	1.2	6.5	3.6	1.9	0.9
	”	1000	83.4	0.2	3.7	1.6	0.7	0.2
300	”	3000	62.3	0.5	5.0	2.4	1.2	0.5
	”	2000	77.2	0.2	3.6	1.6	0.8	0.2
	”	1000	91.4	0.1	1.7	0.7	0.3	0.1

Table 4
Selectivity to alcohols at different reaction conditions.

Temperature (°C)	Pressure (bar)	GHSV (mL/h g_{cat})	X_{CO} (%)	methanol (%)	ethanol (%)	propanol (%)	butanol (%)	pentanol (%)	hexanol (%)	heptanol (%)
250	30	2000	20.3	4.9	13.3	6.2	3.5	1.8	0.5	0.0
	20	”	15.7	10.5	29.4	13.2	8.5	3.3	1.3	0.3
	10	”	11.7	12.0	33.4	13.0	10.5	7.2	3.3	0.5
275	30	”	56.6	4.1	9.3	3.4	1.4	0.4	0.1	0.1
	20	”	35.6	8.0	18.7	6.6	3.8	1.5	0.4	0.1
	10	”	19.4	11.4	25.0	6.5	5.0	4.1	1.7	0.5
300	30	”	78.1	2.2	6.3	2.2	0.9	0.3	0.1	0.0
	20	”	62.2	4.7	12.6	4.2	1.8	0.7	0.2	0.0
	10	”	35.7	6.7	16.7	4.5	2.3	1.9	0.7	0.2
250	30	3000	6.0	5.4	16.0	5.7	4.1	3.4	1.3	0.2
	”	2000	9.2	5.3	13.0	5.1	2.9	1.7	0.5	0.0
	”	1000	26.0	4.3	8.2	2.8	1.4	0.6	0.2	0.1
275	”	3000	28.2	5.3	11.3	4.1	2.1	0.8	0.2	0.1
	”	2000	39.3	4.4	9.5	3.4	1.6	0.6	0.2	0.0
	”	1000	83.4	2.0	4.2	1.4	0.5	0.2	0.0	0.0
300	”	3000	62.3	3.2	7.6	2.5	1.0	0.4	0.1	0.0
	”	2000	77.2	2.2	5.6	1.8	0.7	0.3	0.1	0.0
	”	1000	91.4	0.8	2.5	0.9	0.4	0.1	0.0	0.0

Table 5
α-values and coefficient of determination R^2 for alcohols, alkanes and alkenes at different reaction conditions.

Temperature (°C)	Pressure (bar)	GHSV (mL/h g_{cat})	Alcohols α	R^2	Alkanes α	R^2	Alkenes α	R^2
250	30	2000	0.24	0.974	0.46	0.989	0.40	1.000
	20	”	0.29	0.991	0.47	0.982	0.44	0.996
	10	”	0.30	0.968	0.52	0.855	0.48	0.991
275	30	”	0.28	0.994	0.46	0.967	0.37	0.999
	20	”	0.27	0.998	0.46	0.949	0.42	1.000
	10	”	0.31	0.970	0.49	0.922	0.46	0.999
300	30	”	0.27	0.993	0.46	0.956	0.31	0.997
	20	”	0.25	0.994	0.50	0.921	0.38	0.999
	10	”	0.32	0.982	0.51	0.874	0.44	1.000
250	30	3000	0.31	0.962	0.39	0.964	0.41	0.996
	”	2000	0.31	0.953	0.48	0.978	0.44	0.998
	”	1000	0.29	0.997	0.45	0.978	0.41	1.000
275	”	3000	0.26	0.998	0.44	0.964	0.41	1.000
	”	2000	0.25	0.997	0.45	0.965	0.40	0.999
	”	1000	0.25	0.993	0.44	0.988	0.31	0.996
300	”	3000	0.25	0.996	0.46	0.959	0.37	0.998
	”	2000	0.25	0.997	0.47	0.978	0.33	0.995
	”	1000	0.24	0.993	0.44	0.989	0.31	0.999

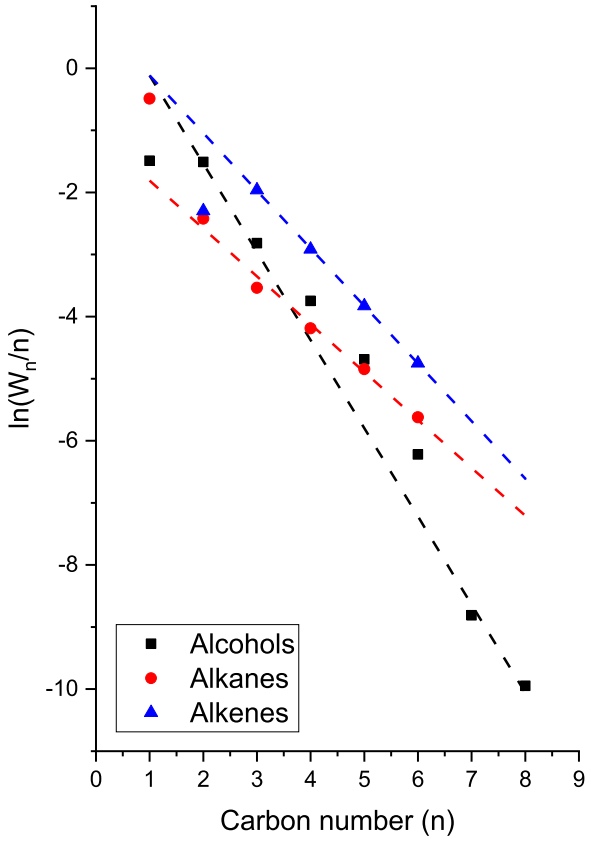

Fig. 13. ASF plots for alcohols, alkanes and alkenes produced at 250 °C, 30 bar and GHSV 2000 g_{cat}^{-1} h^{-1}.

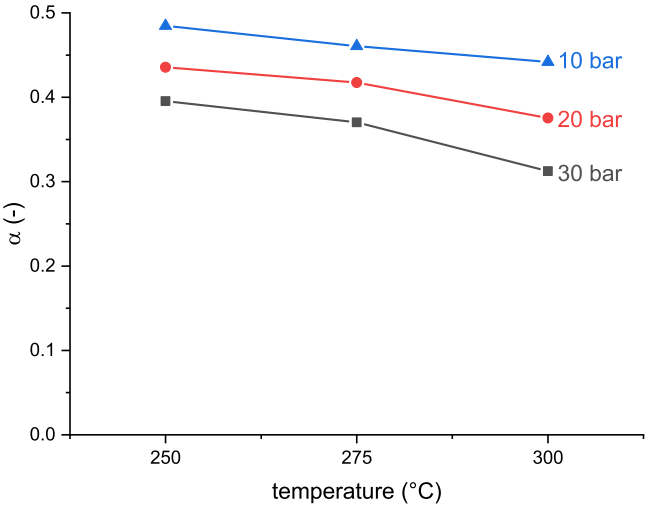

Fig. 14. α-value for alkenes at different reaction pressure as a function of temperature.

reactor, the water in the syngas stream is removed by cooling and condensation. The dried gas stream is heated up to the operation temperature of the alcohol synthesis reactor, 250 °C, before it is fed to the reactor. The model was designed to adjust AEL to provide H_2:CO molar ratio of 2 to the inlet stream to the alcohol synthesis reactor. In the alcohol synthesis reactor, the exothermic reactions forming alcohols, alkenes and alkanes occur. CO conversion and product yields in the process model were based on a selected experiment reported in this study. The operating conditions of the selected experiment were 250 °C and 10 bar, and the resulted CO conversion was 11.7 %. Selectivity of alkanes, alkenes and alcohols is presented in Table 2, Table 3 and Table 4. After the synthesis reactor, the product stream is cooled and gases and liquids are separated by condensation. A case study included CO_2 absorption by monoethanolamine (MEA) and recycling. Such solvent typically gives a relatively high energy consumption compared to more energy efficient solvents like activated methyldiethanalamine, providing, however, reasonable initial estimates for mass balances.

The main operation and performance parameters used in modelling are presented in Table 6. Parametrisation of multistage compressors, other compressors, pumps and heat exchangers were taken from ref. Hannula (2015). CO_2 absorption was performed by monoethanolamine (MEA) absorption process assuming 98 % CO_2 recovery (Tan et al., 2012). For the heat demand of stripping, in-house estimate of 3.5 MJ/kg CO_2 at 120 °C was used, similar as in refs. Knudsen et al. (2009) and Li et al. (2011), and electricity demand of the absorption/stripping process was estimated to be 18 kWh/t CO_2. MEA consumption was assumed to be insignificant in this conceptual study. Electricity demand required for the cooling in the flash separation was estimated assuming the coefficient of performance (COP) of 3.

For the developed concept, 3 different cases were assessed. Case 1 included no by-product gas recycling and no CO_2 removal from the by-product stream. Case 2 included capturing and recycling 98 % of CO_2

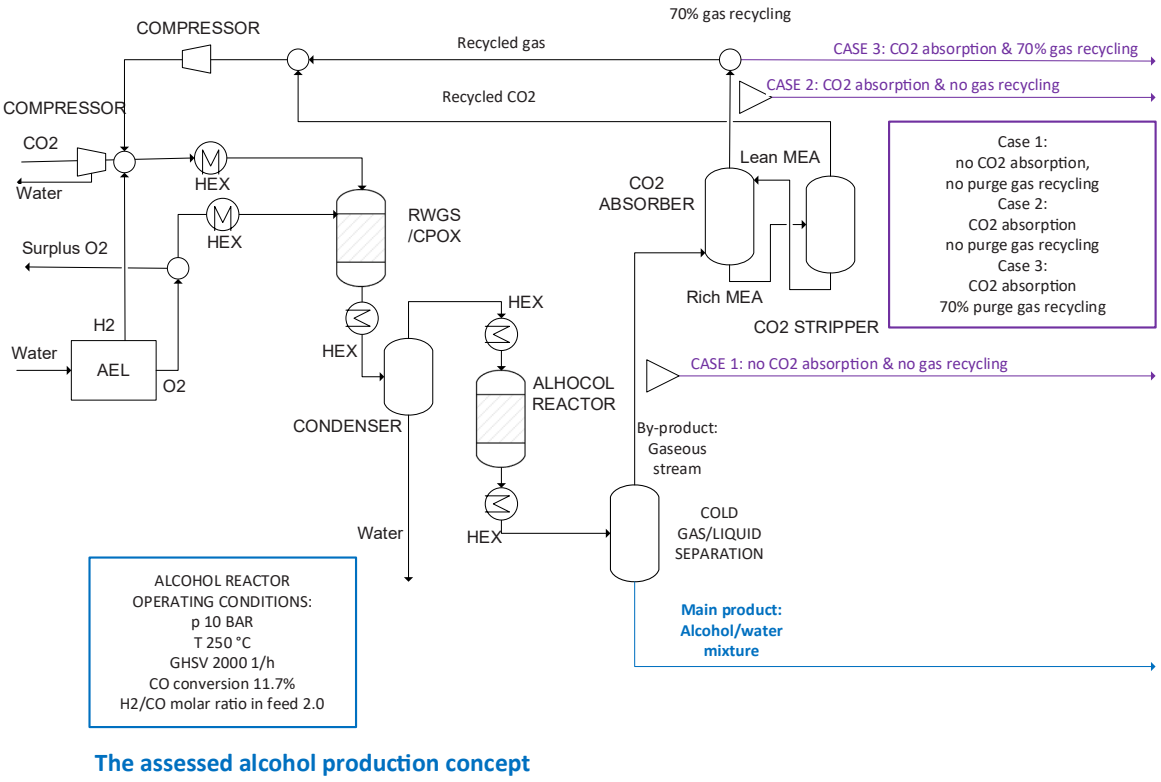

Fig. 15. Flowsheet of the developed concept for alcohol production from CO_2 and water via synthesis gas (AEL refers to alkaline electrolyser, HEX to heat exchanger, MEA to monoethanolamine).

Table 6
Main parameters used for the process model.

Unit	Modelling parameters	Reference
Reverse Water-Gas Shift (RWGS)/ Catalytic Partial Oxidation (CPOX) reactor	Operating conditions 850 °C, at process pressure. Model RGibbs reactor, with possible products defined as CO, CO_2, H_2, H_2O, CH_4, N_2 and solid carbon). Monolith catalyst, Rhodium content 0.5 wt%, carrier Al_2O_3	(Kaisalo et al., 2021; Simell and Hannula, 2023)
Alcohol synthesis reactor	Operating conditions 250 °C, 10 bar. H_2/CO molar ratio in inlet 2.00	Experimental data
Alcohol separation	Gas-liquid separation modelled by a flash, temperature 5 °C Property method CPA	
Alkaline electrolyser (AEL)	State-of-the art electricity demand 50 kWh/kg H_2	(Clean Hydrogen, n. d.)

Table 7
Mass balances for different cases.

Case		1	2	3
Recycling of CO_2		0	98	98
By-product gas recycling	%	0	0	70
IN				
CO_2	t/h	37	25	10
WATER	t/h	32	32	13
Total	t/h	69	57	23
OUT				
Main product alcohol/water mixture	t/h	1.7	1.7	1.7
By-product gaseous stream	t/h	28	16	5.0
Water condensed after CPOX	t/h	13	13	5.4
By-product O_2	t/h	27	27	11
Water condensed from CO_2 compressor	t/h	0.2	0.1	0.02
Total	t/h	69	57	23
Intermediate streams				
Produced H_2	t/h	3.6	3.6	1.5
Syngas to alcohol reactor	t/h	30	30	24

from the by-product stream, using monoethanolamine (MEA) absorption. Case 3 consisted of capturing and recycling 98 % of CO_2 from the by-product stream and 70 % recycling of the rest of the by-product gas.

The Aspen model resulted in a main product, aqueous liquid stream containing water and alcohols, and a by-product, gas stream containing unreacted raw materials CO_2, CO and H_2, some moisture, alkanes and alkenes. Mass balances for the production of 1 t/h alcohols are presented in Table 7. The main product, aqueous solution containing alcohols was similar in all three cases, resulting in total 1.7 t/h alcohol/water mixture and containing approximately 42 wt% of water and approximately 58 wt% of alcohols (Fig. 16). However, the composition of the gaseous by-product stream was different from case to case (Fig. 17). With no recycling, CO_2 content was significant (49 wt%). With CO_2 removal process added, CO_2 content in the product gas stream reduced to insignificant values. Methane content increased with an increasing recycling rate, from case 1 without any recycling (CH_4 1.9 wt%), followed by case 2 with only CO_2 recycling (CH_4 3.5 wt%), to case 3 with recycling both CO_2 and 70 % of the rest gas (CH_4 10 wt%). However, the molar H_2:CO ratio in the by-product gas stream was in all cases equal to 2.

Hydrogen demand was similar for cases 1 and 2, because only CO_2 was recycled (Table 7). However, in case 3 the hydrogen demand was significantly lower due to purge gas recycling to RWGS/CPOX. In addition to recycled unreacted hydrogen, also some hydrogen was formed in steam reforming of recycled hydrocarbons. The mass flow rate of the syngas stream to alcohol reactor was also significantly smaller in case 3 in comparison to cases 1 and 2, although the decrease in the molar flow rate of the same stream in case 3 compared to cases 1 and 2 was

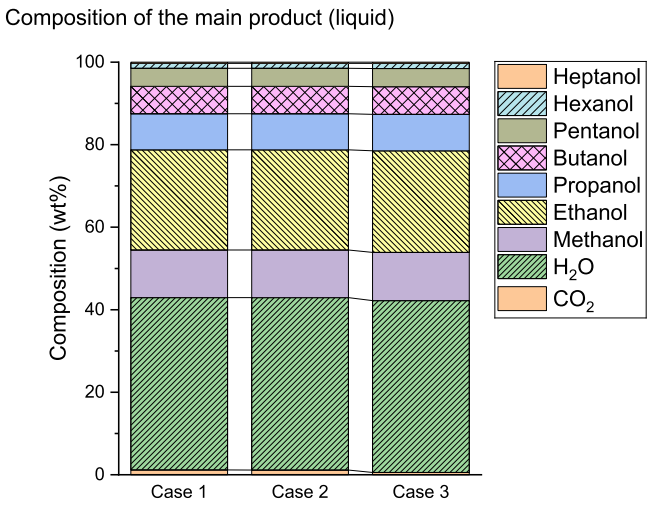

Fig. 16. Weight based composition of the main product (liquid) for the 3 cases.

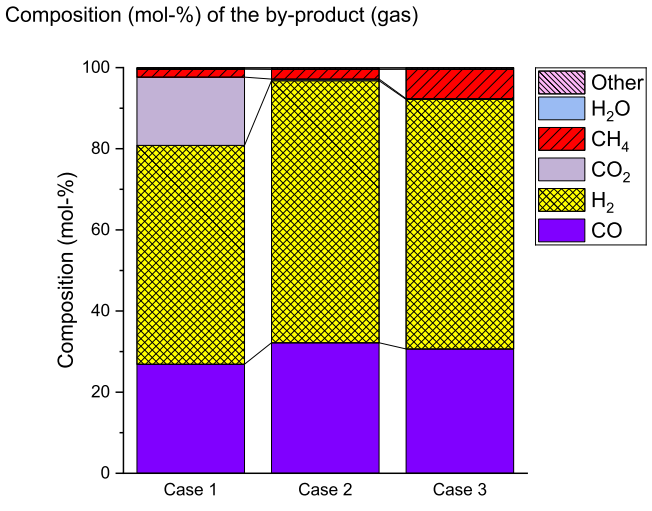

Fig. 17. Molar composition of the by-product (gases) for the 3 cases.

only 4 %, mainly due to a slightly increased CO content (from 28 to 29 mol%). The lower mass flow rate in case 3 derived mainly from lower CO_2 content (15 mol% in case 1 and case 2, 7 mol% in case 3) and increased CH_4 content (2 mol% in case 1 and case 2, 6 mol% in case 3).

The electricity demand was 181 MW for cases 1 and 2, and 77 MW for case 3 due to lower hydrogen demand. In all cases 99 % of the electricity demand was related to the electrolyser emphasizing that more efficient electrolysis will drive the costs significantly down. Pinch analysis showed for case 1 cold utility of 14 MW and hot utility of 0 MW. In case 2 cold utility demand decreased to 4 MW and hot utility increased to 2 MW due to the heat demand of CO_2 stripping after adsorption. In case 3, the heat demand of CO_2 stripping was significantly lower compared to case 2 due to purge gas recycling, with the pinch analysis resulting in hot utility demand of 0 MW and cold utility demand of 2 MW.

Further processing options were developed but not evaluated quantitatively (Fig. 18). However, they are discussed here. The alcohol fraction in general may be utilized in many processes, but here it was considered for production of sustainable aviation fuel (SAF). The processing route would include alcohols (except methanol) dehydration to olefins, followed by separation of water and methanol. The remaining C_2-C_6 olefins would be first oligomerised and then hydrogenated (hydrogen addition) (Chang et al., 1993; O'Connor and Kojima, 1990; Wang et al., 2016). The resulting mixture would be fractioned to SAF and lighter hydrocarbons to be used as e.g. road gasoline. The design is similar to the biobased alcohol to jet process (Vela-García et al., 2020).

The experimental work showed that the fatty alcohol reaction had low conversion combined with high selectivity and vice versa. If aiming for higher conversion, the selectivity decreases. Obviously it will not be economically feasible to have once-through operation with such a low conversion. Recycling improves the overall yield, but reasonable yields would require very high recycling rates. However, as the resulting gas stream contains H_2:CO molar ratio of 2, it is a potential feed stream to another processes (Fig. 17). Thus, the by-product gas stream could be used as a feed stream for example to FT process or to a methanol synthesis process.

The FT process produces alkanes and alkenes from syngas, and the FT product stream could be fractionated and refined to fuels and/or chemicals. Heating the by-product gas stream from ambient temperature to FT operation temperature (150–300 °C) would be required (de Klerk, 2011). Pressurization may also be needed if the operation pressure of the selected FT process is above 10 bar. The benefits of using the by-product gas stream as a feed stream to FT synthesis include the often desired H_2:CO ratio in the feed, 2.0 (de Klerk, 2011), in all cases. Based on the published kinetic studies regarding cobalt catalysed FT (Keyvanloo et al., 2016; Lillebø et al., 2017) the reaction rate in the FT inlet decreases due to increase in the inert content, whereas selectivity to C_{5+} remains relatively the same and the selectivity to methane decreases. Thus, the low inert content emphasizes a potential to reach the higher conversion of CO above 70 % (Steynberg and Dry, 2004; Wolf et al., 2019). Both cases 2 and 3 have very low CO_2 and other inert content (below 8 mol%), however in case 1 the conversion may be reduced due to a higher CO_2 content (17 mol% CO_2).

Methanol may be another option to be produced from the synthesis gas. It may be used as a chemical intermediate or as fuel, but it may also be converted to olefins and further for example to aviation fuel or chemicals. Methanol synthesis is exothermic and equilibrium limited, but efficient gas recycling results nearly in 100 % conversion (Basile and Dalena, 2018; Sehested, 2019). The commercial operating conditions are typically 200–300 °C and at 50–100 bar (Sehested, 2019). For methanol synthesis from syngas, the optimal H_2:CO feed ratio based on the reaction equation would be 2:1. However, currently used copper catalysts are active also for WGS reaction (formation of CO_2) and able to convert some CO_2 to methanol (H_2:CO_2 reaction ratio is 3:1) (de Klerk, 2014). Thus, typically the preferred H_2:CO ratio is above 2 for copper catalysts (de Klerk, 2014) or Module number $(n_{H2}\text{-}n_{CO2})/(n_{CO}+n_{CO2})$ based on molar flow rates close to 2 (Sehested, 2019). Considering the composition of the product gas, cases 2 and 3 would provide a suitable feed stream to the methanol synthesis if minor additional H_2 would be added to increase the H_2:CO ratio. Case 1 could also give a suitable feed, with the benefit that CO_2 is converted to methanol along with the syngas, if a larger hydrogen addition is available. A higher additional hydrogen stream would be needed to maximise the methanol yield for case 1 compared to cases 2 and 3. The drawback of case 1 is that CO_2 content in the feed stream results in a loss of some H_2, which forms water according to the reaction equation.

4. Conclusions

An 11 %-CuFeCoK/SiO_2 catalyst was used for synthesis of higher alcohols from syngas. Different reaction conditions were tested namely, temperature 250 – 300 °C, pressure 10 – 30 bar, as well as different residence times by varying the GHSV from 1000 to 3000 mL h^{-1} g_{cat}^{-1} the H_2:CO ratio was kept constant with a value of 2. It was found that the selectivity to higher alcohols decreased with increasing CO conversion. However, at low CO conversion it was possible to obtain ethanol as the main product with a selectivity as high as 33.4 %.

The main outcome of the experimental work with CuFeCoK/SiO2 is that while there are differences in selectivity to alkanes, alkenes and higher alcohols for different catalysts reported in the literature, the main

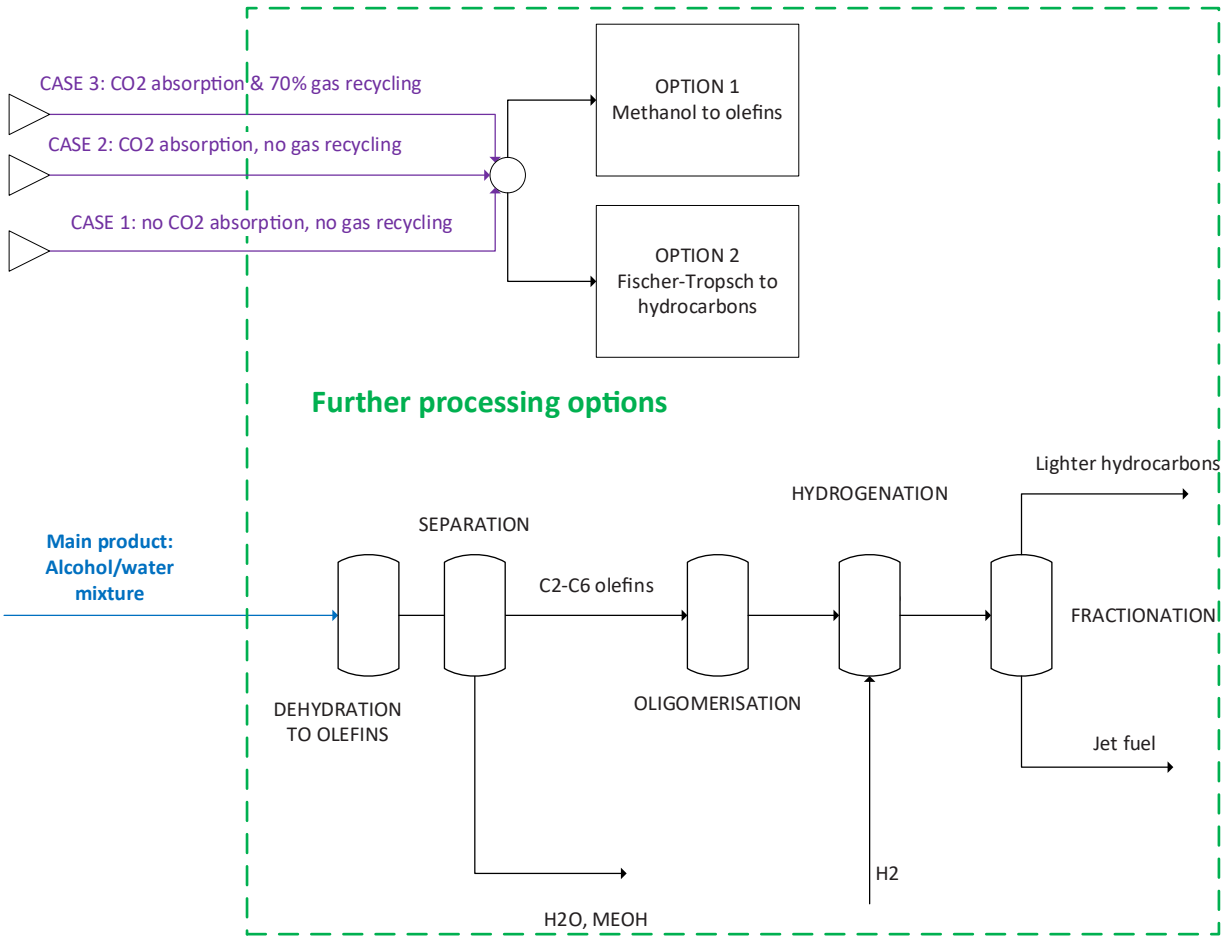

Fig. 18. Further processing options for both alcohol/water mixture and for the gaseous by-product.

trends remain, namely high selectivity to alcohols at low conversion, a clear decline in selectivity to alcohols when the conversion increases, the positive influence of pressure on reactivity as well as the reaction orders in the reactants.

The experimental work was a starting point to design a process concept to produce higher alcohols as the main product from CO_2 and water. The designed concept was modelled using Aspen + steady state modelling software, considering a gaseous stream as a by-product. The modelling work utilized the experimental results of the alcohol synthesis from the first part of this publication.

Process-wise, the main guiding conclusion from the experimental work is that high selectivity to alcohols can be achieved at a relatively low CO conversion, thus either gas recycling should be considered or in the case of once-through production of higher alcohols, unconverted syngas should be used for making valuable chemicals and fuels, e.g. in the Fischer-Tropsch or methanol synthesis.

Due to the combination of high selectivity to alcohols with a relatively low CO conversion, several syngas utilization or recycling options were considered to maximize the carbon utilization efficiency. Recycling both 98 % of CO_2 by absorption and then 70 % of the gaseous by-product resulted in over 50 % decrease in electricity demand and 20 % decrease in the synthesis reactor volume, when comparing to once-through operation. In addition to the concept development for the alcohol synthesis, the conceptual design work addressed qualitatively, how the produced alcohols could be converted to jet fuel and how the gaseous by-product could be utilised. Regarding the downstream process integration, the mass and energy balances showed that the by-product gas had both a low content of the inert and a H_2:CO ratio of 2, which makes it a suitable feed for the Fischer-Tropsch synthesis. When considering methanol synthesis, a minor hydrogen addition would be required for high gas recycling, while a larger hydrogen addition is required for the once-through operation. Thus, the Fischer-Tropsch synthesis or methanol synthesis could be integrated as a downstream process for the gaseous by-product stream in the higher alcohol plant.

CRediT authorship contribution statement

Dmitry Yu. Murzin: Writing – review & editing, Supervision, Project administration, Methodology, Funding acquisition, Conceptualization. **Juha Lehtonen:** Supervision, Project administration, Methodology, Investigation. **Atte Aho:** Writing – original draft, Methodology, Investigation. **Niko Heikkinen:** Investigation. **Hannu I. Mikkonen:** Methodology, Investigation. **Anssi Peuronen:** Investigation. **Marjut Suomalainen:** Investigation. **Mika Lastusaari:** Supervision. **Kari Eränen:** Project administration, Methodology, Investigation. **Irina Simakova:** Investigation. **Päivi Mäki-Arvela:** Supervision.

Declaration of Competing Interest

The authors declare that they have no known competing financial interests or personal relationships that could have appeared to influence the work reported in this paper.

Acknowledgments

This work is part of the activities of the Johan Gadolin Process Chemistry Centre at Åbo Akademi University. Funding from Business

Finland through the SynJet project is greatly acknowledged.

References

Aho, A., Lind, N., Virtanen, P., Mäki-Arvela, P., Eränen, K., Granroth, S., Korpelin, V., Honkala, K., Russo, V., Simakova, I., Murzin, D.Yu, 2024. Influence of Cu:Fe ratio in synthesis of higher alcohols from syngas over CuFeCoK/attapulgite catalysts. Appl. Catal. O Open 193, 206972. https://doi.org/10.1016/j.apcato.2024.206972.

Basile, A., Dalena, F. (Eds.), 2018. Methanol: Science and Engineering, Elsevier B.V. Elsevier B.V., Amsterdam.

Chang, C.D., Hellring, S.D., Striebel, R.F., 1993. Process for hydrogenating alkenes in the presence of alkanes and a heterogeneous catalyst. US5227552A.

Chen, J., Yang, C., 2019. Thermodynamic equilibrium analysis of product distribution in the Fischer–Tropsch process under different operating conditions. ACS Omega 4, 22237–22244. https://doi.org/10.1021/acsomega.9b03707.

Chen, Y., Ma, L., Zhang, R., Ye, R., Liu, W., Wei, J., Ordomsky, V.V., Liu, J., 2022. Carbon-supported fe catalysts with well-defined active sites for highly selective alcohol production from Fischer-Tropsch synthesis. Appl. Catal. B Environ. 312, 121393. https://doi.org/10.1016/j.apcatb.2022.121393.

Clean Hydrogen, n.d. Clean Hydrogen Joint Undertaking. 2022. Strategic Research and Innovation Agenda 2021-2027. [WWW Document]. URL ⟨https://www.clean-hydrogen.europa.eu/knowledge-management/strategy-map-and-key-performance-indicators/clean-hydrogen-ju-sria-key-performance-indicators-kpis_en⟩ (Accessed 4.30.25).

de Klerk, A., 2014. Chapter 12 - transport fuel: Biomass-, Coal-, Gas- and Waste-to-Liquids processes. In: Letcher, T.M. (Ed.), Future Energy (Second Edition). Elsevier, Boston, pp. 245–270. https://doi.org/10.1016/B978-0-08-099424-6.00012-0.

de Klerk, A., 2011. Fischer Tropsch refining. Wiley-VCH Verlag GmbH & Co. KGaA.

de la Peña O'Shea, V.A., Alvarez-Galvan, M.C., Campos-Martin, J.M., Fierro, J.L.G., 2005. Strong dependence on pressure of the performance of a Co/SiO2 catalyst in Fischer–Tropsch slurry reactor synthesis. Catal. Lett. 100, 105–116. https://doi.org/10.1007/s10562-004-3096-7.

Degen, T., Sadki, M., Bron, E., König, U., Nénert, G., 2014. The highscore suite. Powder Diffr. 29, S13–S18. https://doi.org/10.1017/S0885715614000840.

Gates-Rector, S., Blanton, T., 2019. The powder diffraction file: a quality materials characterization database. Powder Diffr. 34, 352–360. https://doi.org/10.1017/S0885715619000812.

Göbel, C., Schmidt, S., Froese, C., Bujara, T., Viktor Scherer, Muhler, M., 2021. The steady-state kinetics of CO hydrogenation to higher alcohols over a bulk Co-Cu catalyst. J. Catal. 394, 465–475. https://doi.org/10.1016/j.jcat.2020.10.017.

Gong, N., Wu, Y., Ma, Q., Tan, Y., 2023. A simple strategy stabilizing for a CuFe/SiO2 catalyst and boosting higher alcohols' synthesis from syngas. Catalysts 13, 237. https://doi.org/10.3390/catal13020237.

Hannula, I., 2015. Synthetic fuels and light olefins from biomass residues, carbon dioxide and electricity: Dissertation (Doctor's thesis), VTT Technical Research Centre of Finland Ltd. VTT Technical Research Centre of Finland Ltd.

He, M., Luo, M., Fang, P., 2006. Characterization of CuO species and thermal Solid-Solid interaction in CuO/CeO2-Al2O3 catalyst by In-Situ XRD, Raman spectroscopy and TPR. J. Rare Earths 24, 188–192. https://doi.org/10.1016/S1002-0721(06)60091-4.

Hong, Z., Wang, J., Gao, Z., Huang, W., 2024. Tuning CuO crystallite size by different solvents for higher alcohols synthesis from syngas over CuZnAl catalyst. Int. J. Hydrog. Energy 56, 1032–1037. https://doi.org/10.1016/j.ijhydene.2023.12.292.

Hornés, A., Bera, P., Cámara, A.L., Gamarra, D., Munuera, G., Martínez-Arias, A., 2009. CO-TPR-DRIFTS-MS *in situ* study of CuO/Ce1−*x*TbxO2−*y* ($x = 0$, 0.2 and 0.5) catalysts: support effects on redox properties and CO oxidation catalysis. J. Catal. 268, 367–375. https://doi.org/10.1016/j.jcat.2009.10.007.

Kaisalo, N., Simell, P., Frilund, C., Vidal, V.F., Hannula, I., 2021. Method and Apparatus for Producing Carbon Monoxide. US2021246034A1.

Keyvanloo, K., Lanham, S.J., Hecker, W.C., 2016. Kinetics of Fischer-Tropsch synthesis on supported cobalt: effect of temperature on CO and H2 partial pressure dependencies. Catal. Today C1 Catal. Chem. 270, 9–18. https://doi.org/10.1016/j.cattod.2016.03.019.

Khunphonoi, R., Khemthong, P., Luadthong, C., Kuboon, S., Kongmark, C., Viriya-empikul, N., Kidkhunthod, P., Pinitsoontorn, S., Faungnawakij, K., 2022. Correlating the effect of preparation methods on the structural and magnetic properties, and reducibility of $CuFe_2O_4$ catalysts. RSC Adv. 12, 15526–15533. https://doi.org/10.1039/D2RA01708C.

Knudsen, J.N., Jensen, J.N., Vilhelmsen, P.-J., Biede, O., 2009. Experience with CO2 capture from coal flue gas in pilot-scale: testing of different amine solvents. Energy Procedia Greenh. Gas. Control Technol. 9 (1), 783–790. https://doi.org/10.1016/j.egypro.2009.01.104.

Li, H., Haugen, G., Ditaranto, M., Berstad, D., Jordal, K., 2011. Impacts of exhaust gas recirculation (EGR) on the natural gas combined cycle integrated with chemical absorption CO2 capture technology. Energy Procedia 10th Int. Conf. Greenh. Gas. Control Technol. 4, 1411–1418. https://doi.org/10.1016/j.egypro.2011.02.006.

Li, Y., Gao, W., Peng, M., Zhang, J., Sun, J., Xu, Y., Hong, S., Liu, Xi, Liu, Xingwu, Wei, M., Zhang, B., Ma, D., 2020. Interfacial Fe5C2-Cu catalysts toward low-pressure syngas conversion to long-chain alcohols. Nat. Commun. 11, 61. https://doi.org/10.1038/s41467-019-13691-4.

Lillebø, A., Rytter, E., Blekkan, E.A., Holmen, A., 2017. Fischer–Tropsch synthesis at high conversions on Al2O3-supported co catalysts with different H2/CO levels. Ind. Eng. Chem. Res. 56, 13281–13286. https://doi.org/10.1021/acs.iecr.7b01801.

Lind, N., Aho, A., Eränen, K., Virtanen, P., Simakova, I., Mäki-Arvela, P., Murzin, D.Yu, 2024. Transformation of syngas to valuable oxygenated products over Rh-MnOx/SiO2, Rh-Co/ZrO2 and Rh-Cu/ZrO2 catalysts. Appl. Catal. A Gen. 683, 119852. https://doi.org/10.1016/j.apcata.2024.119852.

Liu, B., Li, Y., Duan, Y., Ding, T., Tang, Y., Zheng, C., 2019. Effect of supports on performance of Cu–Fe based catalysts for higher alcohols synthesis from syngas. React. Kinet. Mech. Cat. 128, 695–706. https://doi.org/10.1007/s11144-019-01667-w.

Liu, G., Fang, H., Wang, G., Liu, N., Liu, J., Huang, L., Liang, X., Yuan, Y., 2021. Dispersion of Rh–WxC nanocomposites on carbon nanotubes by one-pot carburization for synthesis of higher alcohols from syngas. Fuel 305, 121533. https://doi.org/10.1016/j.fuel.2021.121533.

Lu, Y., Yu, F., Hu, J., Liu, J., 2012. Catalytic conversion of syngas to mixed alcohols over Zn-Mn promoted Cu-Fe based catalyst. Appl. Catal. A Gen. 429–430, 48–58. https://doi.org/10.1016/j.apcata.2012.04.005.

Luk, H.T., Mondelli, C., Ferré, D.C., Stewart, J.A., Pérez-Ramírez, J., 2017. Status and prospects in higher alcohols synthesis from syngas. Chem. Soc. Rev. 46, 1358–1426. https://doi.org/10.1039/C6CS00324A.

Luk, H.T., Mondelli, C., Mitchell, S., Curulla Ferré, D., Stewart, J.A., Pérez–Ramírez, J., 2019. Impact of carrier acidity on the conversion of syngas to higher alcohols over zeolite-supported copper-iron catalysts. J. Catal. 371, 116–125. https://doi.org/10.1016/j.jcat.2019.01.021.

Luk, H.T., Mondelli, C., Mitchell, S., Siol, S., Stewart, J.A., Curulla Ferré, D., Pérez-Ramírez, J., 2018. Role of carbonaceous supports and potassium promoter on higher alcohols synthesis over copper–iron catalysts. ACS Catal. 8, 9604–9618. https://doi.org/10.1021/acscatal.8b02714.

Luo, M., Hamdeh, H., Davis, B.H., 2009. Fischer-Tropsch synthesis: catalyst activation of low alpha iron catalyst. Catal. Today Catal. Chem. Synth. Fuels Chem. Petrochem. 140, 127–134. https://doi.org/10.1016/j.cattod.2008.10.004.

Mäki-Arvela, P., Aho, A., Simakova, I., Yu. Murzin, D., 2022. Sustainable aviation fuel from syngas through higher alcohols. ChemCatChem 14, e202201005. https://doi.org/10.1002/cctc.202201005.

Maximov, V.V., Permyakov, E.A., Dorokhov, V.S., Wang, A., Kooyman, P.J., Kogan, V.M., 2020. Effect of promoter nature on synthesis gas conversion to alcohols over (K)MeMoS2/Al2O3 catalysts. ChemCatChem 12, 1443–1452. https://doi.org/10.1002/cctc.201901698.

Murzin, D.Yu, 2019. On apparent activation energy of structure sensitive heterogeneous catalytic reactions. Catal. Lett. 149, 1455–1463. https://doi.org/10.1007/s10562-019-02772-0.

O'Connor, C.T., Kojima, M., 1990. Alkene oligomerization. Catal. Today 6, 329–349. https://doi.org/10.1016/0920-5861(90)85008-C.

Sehested, J., 2019. Industrial and scientific directions of methanol catalyst development. J. Catal. 371, 368–375. https://doi.org/10.1016/j.jcat.2019.02.002.

Simell, P., Hannula, I., 2023. Method and apparatus for producing product gas and use. US2023373784A1.

Sonal, Pant, K.K., Upadhyayula, S., 2020. An insight into the promotional effect on Fe-Co bimetallic catalyst in the fischer tropsch reaction: a DRIFTS study. Fuel 276, 118044. https://doi.org/10.1016/j.fuel.2020.118044.

Steynberg, A., Dry, M., 2004. FT catalysts (Eds.). Fischer-Tropsch Technology, Studies in Surface Science and Catalysis. Elsevier Science, pp. 533–600 (Eds.).

Subramanian, N.D., Kumar, C.S.S.R., Watanabe, K., Fischer, P., Tanaka, R., Spivey, J.J., 2012. A DRIFTS study of CO adsorption and hydrogenation on Cu-based core–shell nanoparticles. Catal. Sci. Technol. 2, 621–631. https://doi.org/10.1039/C2CY00413E.

Tan, L.S., Lau, K.K., Bustam, M.A., Shariff, A.M., 2012. Removal of high concentration CO2 from natural gas at elevated pressure via absorption process in packed column. J. Nat. Gas. Chem. 21, 7–10. https://doi.org/10.1016/S1003-9953(11)60325-3.

Vela-García, N., Bolonio, D., Mosquera, A.M., Ortega, M.F., García-Martínez, M.-J., Canoira, L., 2020. Techno-economic and life cycle assessment of triisobutane production and its suitability as biojet fuel. Appl. Energy 268, 114897. https://doi.org/10.1016/j.apenergy.2020.114897.

Vikram, S., Aho, A., Mäki-Arvela, P., Murzin, D.Yu, 2025. Process optimization and techno-economic assessment of commercial scale synthesis of fatty alcohols from biomass-based syngas. Chem. Eng. Res. Des. 219, 34–42. https://doi.org/10.1016/j.cherd.2025.05.055.

Wang, W.-C., Tao, L., Markham, J., Zhang, Y., Tan, E., Batan, L., Warner, E., Biddy, M., 2016. Review of biojet fuel conversion technologies. National Renewable Energy Laboratory (NREL), Golden, CO (United States). https://doi.org/10.2172/1278318.

Wolf, M., Gibson, E.K., Olivier, E.J., Neethling, J.H., Catlow, C.R.A., Fischer, N., Claeys, M., 2019. Water-induced formation of cobalt-support compounds under simulated high conversion Fischer–Tropsch environment. ACS Catal. 9, 4902–4918. https://doi.org/10.1021/acscatal.9b00160.

Wu, Y., Xie, H., Tian, S., Tsubaki, N., Han, Y., Tan, Y., 2015. Isobutanol synthesis from syngas over K–Cu/ZrO2–La2O3(x) catalysts: effect of La-loading. J. Mol. Catal. A Chem. 396, 254–260. https://doi.org/10.1016/j.molcata.2014.10.003.

Xiao, K., Bao, Z., Qi, X., Wang, X., Zhong, L., Fang, K., Lin, M., Sun, Y., 2013. Structural evolution of CuFe bimetallic nanoparticles for higher alcohol synthesis. J. Mol. Catal. A Chem. 378, 319–325. https://doi.org/10.1016/j.molcata.2013.07.006.

Zeng, Z., Li, Z., Guo, S., Lv, J., Huang, S., Wang, Y., Ma, X., 2021. Janus Au–Fe2.2C catalyst for direct conversion of syngas to higher alcohols. ACS Sustain. Chem. Eng. 9, 11258–11268. https://doi.org/10.1021/acssuschemeng.1c04263.

Zheng, S., Liu, Y., Li, J., Shi, B., 2007. Deuterium tracer study of pressure effect on product distribution in the cobalt-catalyzed Fischer–Tropsch synthesis. Appl. Catal. A Gen. 330, 63–68. https://doi.org/10.1016/j.apcata.2007.07.010.